The Ross Ice Shelf: Glaciology and Geophysics
Antarctic Research Series, Volume 42, Paper 4, Pages 87-108

SEISMIC STUDIES ON THE GRID EASTERN HALF OF THE ROSS ICE SHELF: RIGGS III AND RIGGS IV

Donald G. Albert

U.S. Army Cold Regions Research and Engineering Laboratory
Hanover, New Hampshire 03755

Charles R. Bentley

Geophysical and Polar Research Center, University of Wisconsin
Madison, Wisconsin 53706

Abstract. Seismic P wave refraction experiments at three locations on the Ross Ice Shelf during 1976-1977 (RIGGS III) and 1977-1978 (RIGGS IV) reveal that the velocity increases monotonically in the firn from about 500 m s^{-1} at the surface to about 3800 m s^{-1} at a depth of 60 m. Maximum P wave velocities measured at four locations on the ice shelf show a large range of values primarily indicative of lateral inhomogeneities, but perhaps also resulting from anisotropy. The ice and water column thicknesses at station J9DC determined from reflection shooting are 414 ± 2 m and 244 ± 6 m, respectively. These values agree well with values of 417 ± 2 m and 240 ± 2 m measured in a borehole at that location. Water depths for 89 additional stations were determined using seismic reflections from the ocean floor together with ice thicknesses measured by radar and seismic techniques. Systematic differences that appear between ice thicknesses measured by the two techniques on RIGGS IV but not on RIGGS III most likely reflect an unrecognized systematic error in measurement. The amplitudes of ocean bottom and ice shelf bottom reflections at one station have been used, together with standard velocity-density curves, to calculate a density of 1.90 ± 0.12 Mg m^{-3} and a velocity of 1.72 ± 0.06 km s^{-1} in the uppermost sediment. Rayleigh, Love, and leaky-mode surface waves were recorded in experiments at station Q13. Theoretical surface wave dispersion curves calculated from measured body wave velocities give values higher than those observed. Dispersion curves calculated from several other velocity models indicate that agreement for the higher-mode surface waves can be obtained by modifying the S wave velocities in the upper few meters of the ice wherein they have not been determined accurately by the refraction shooting. Anisotropy may account for the differences between the observed and calculated values in the fundamental modes.

Contents

Introduction

The experiments discussed in this paper were carried out during the Ross Ice Shelf Geophysical and Glaciological Survey (RIGGS) field seasons from October 1976 to February 1977 (RIGGS III) and from December 1977 through January 1978 (RIGGS IV). Geophysical measurements were made at 94 stations, covering the grid eastern half of the Ross Ice Shelf. For a summary of RIGGS, see paper 1 of this volume [Bentley, 1984].

Seismic velocities in the ice shelf increase with depth to about 100 m because of compaction and recrystallization of the snow layers. Below this depth, the velocity decreases gradually downward because of increasing temperature [Crary et al., 1962a]. Consequently, refracted waves may be used to investigate the snow and firn only to a depth of about 80 m; only reflections can yield information about the lower part of the ice shelf. Seismic wave attenuation is much lower in ice than in most other materials encountered in seismic work, so high-frequency energy propagates easily over long distances with little loss. Signal frequencies greater than 100 Hz are common in reflection shooting on ice sheets, and ocean bottom reflections with frequencies of 200 Hz are routinely recorded from beneath ice shelves. These frequencies are substantially greater than those normally used in seismic

prospecting (typically 8-80 Hz).

Here we report on three types of seismic experiments: (1) short-refraction shooting was used to determine the compressional (P) and shear (S) wave velocities and, from the P wave velocities, the density as a function of depth in the upper part of the shelf; (2) surface wave studies provided an independent check on the refraction results and also gave an indication of anisotropy in the upper layers of the firn; (3) seismic reflections were used to measure the thickness of the water layer and in many places the ice thickness also. Radar sounding normally is the primary means of determining ice thickness, but during RIGGS III an equipment failure meant that the field party operating out of the base camp at C-16 lacked a radar system for much of the season. As a result, only seismic measurements were available at 21 stations in the grid northeastern quadrant of the ice shelf.

Recording was done with 24-channel SIE model RA-49R seismograph systems modified to record frequencies up to 500 Hz. An SIE R-6 oscillograph was used to record the shots; no tape recording system was available. The shot instant was recorded on a separate channel, either by a direct connection from the shot box or by radio transmission. Normal seismic shooting procedures were used; either hammer blows or explosives (blasting caps at short distances, 0.4-kg charges at longer distances) served as the source. Shot holes up to 15 m deep were drilled by hand in the ice using a SIPRE auger. Both horizontal and vertical geophones were used, usually with one geophone per channel.

Short-Refraction Shooting

The purpose of short-refraction shooting is to investigate the properties of the upper layers of the ice sheet. By measuring the travel time of a seismic wave as a function of shot-receiver distance, the velocity as a function of depth can be determined. A very useful empirical equation formulated by Kohnen [1972] gives the density of the ice from the P wave velocity. If S wave velocities are also determined, the elastic constants of the ice can be calculated.

Lines to record P waves, SV waves (shear waves polarized in the plane of propagation), and SH waves (shear waves transversely polarized) were shot at the base camps C-16, J9DC, and Q13; short P wave lines were shot at the 2-day stations H13, M14, and N19 during RIGGS III and at O11, O19, and R16 during RIGGS IV (see Figure 1). The detailed results of the RIGGS IV refraction experiments are compiled in Appendix A; those from RIGGS III are presented by Kirchner [1978] [Kirchner et al., 1979; Kirchner and Bentley, this volume]. (All appendix material is on microfiche, enclosed in a pocket inside the back cover of this minibook.) Robertson [1975] [Robertson and Bentley, this volume] and Crary et al. [1962a, b] have reported on previous refraction work on the ice shelf.

For the refraction experiments discussed here, the detecting spread consisted of 24 vertically oriented geophones set at 2-m intervals. The spread was left unchanged, while the shot point was moved from the end of the spread out to a distance of 400 m in 40-m increments. This shooting procedure results in a 6-m overlap for adjacent shots. At station R16 an additional shot was set off 710 m from the farthest geophone. At some locations, direct arrivals from reflection shots with a geophone spacing of 30 m were used to give additional travel times for longer distances. The time breaks for all shots were recorded on a separate channel through a wire directly connecting the shot box with the recording unit. Typical seismic refraction records are shown in Figures 2 and 3. (Ice bottom and water bottom reflections do not appear on these records because of small charge sizes at short distances and no low-cut filtering on any refraction records.)

A larger reproduction of one record is shown in Figure 4. This seismogram is from a 1 lb (0.4 kg) charge in a 1-m hole, 336 m from the nearest geophone. The first arrival at each geophone is the refracted P wave (P_1), followed by a series of refracted multiples (P_m) that have been reflected m-1 times from the ice-air interface. The velocity of these waves across the detecting spread at distance x is equal to the velocity of a P_1 arrival at x/m. The shear wave arrival (S) is next on the record, followed by higher-mode Rayleigh waves (R_H) and the fundamental mode Rayleigh wave (R_1). The Rayleigh waves are discussed in a later section.

The first arrival times at each geophone were read from the seismograms, using a 7X magnifier, to a precision of 0.1 ms and an accuracy of 0.2-0.3 ms. A computer program was then used to smooth the travel times, t(x), by fitting them to an equation of the form (see Kirchner and Bentley [this volume] for explanation and discussion)

$$t(x) = t_1(1 - e^{-a_1 x}) + t_2(1 - e^{-a_2 x}) + v_m^{-1} \qquad (1)$$

where a_1, a_2, t_1, t_2, and v_m^{-1} are parameters chosen for the best least squares fit. Table 1 shows the parameters determined for the RIGGS IV P wave refraction experiments. An example of a P wave travel time plot (from station R16) is shown in Figure 5. The best fit regression line fits the data points

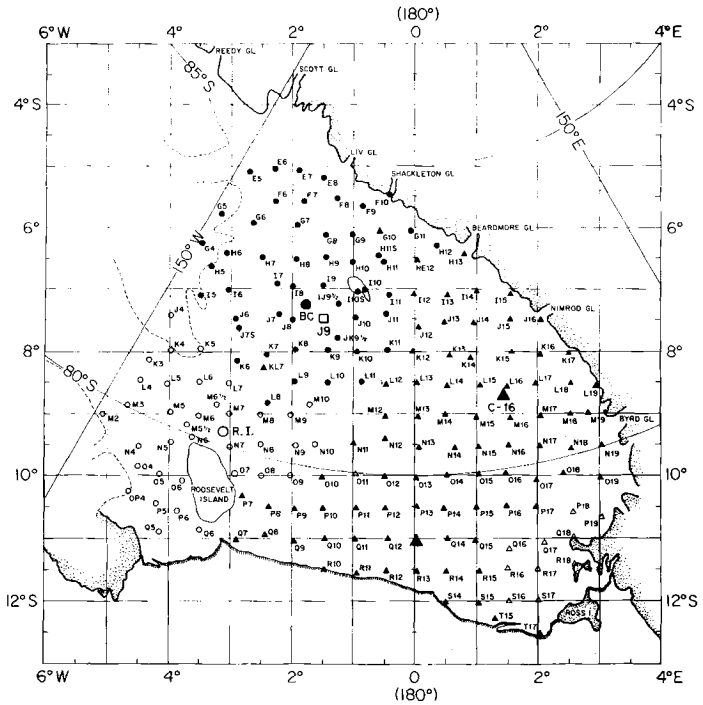

Fig. 1. Map of RIGGS stations [from Bentley, 1984]. Stations occupied during RIGGS III and IV are indicated by solid triangles and open triangles, respectively. In the rectangular grid coordinate system shown, meridians are parallel to the Greenwich meridian, with grid north toward Greenwich. The origin of the system is at the South Pole, and 1° of grid latitude or longitude equals 1° of geographic latitude.

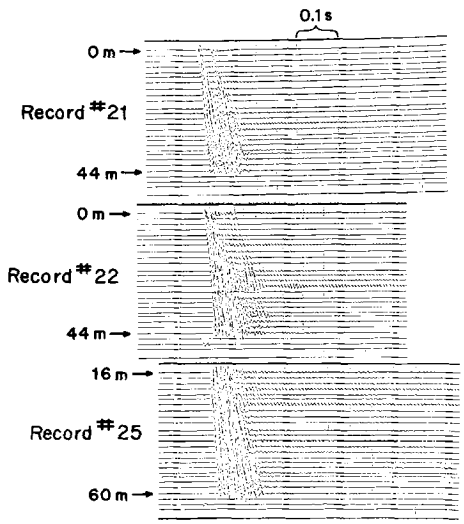

Fig. 2. Sample P wave short-refraction records at small separations, from station R16. Geophones were 2 m apart; distances for closest and most distant geophone for each record are marked. The energy source for each record was a hammer blow.

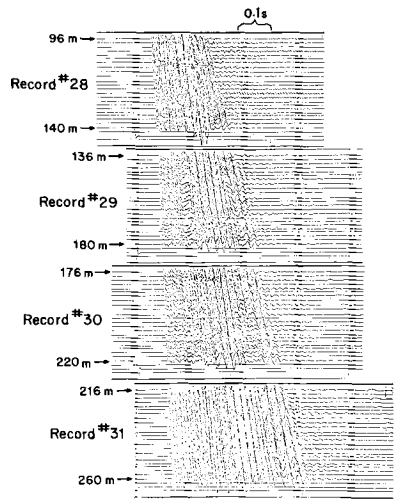

Fig. 3. Sample P wave short-refraction records at relatively large separations, from station R16. Geophones were 2 m apart; distances for closest and most distant geophone for each record are marked. The energy source for each record was a 0.4-kg charge in a 1-m hole.

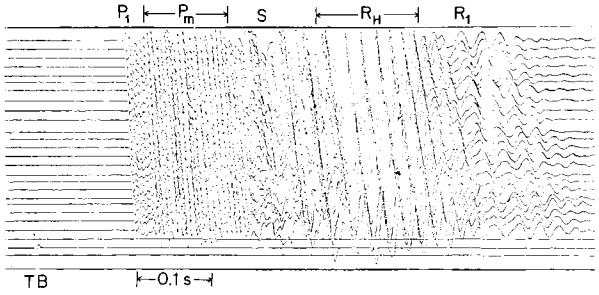

Fig. 4. Enlargement of a short-refraction record (record 39) from station R16. The geophone interval was 2 m, the minimum distance was 336 m, and the energy source was a 0.4-kg charge in a 1-m hole.

extremely closely (the line is not drawn in the figure because it would obscure the points), as is necessary if equation (1) is satisfactorily to represent the observed travel times. The standard deviation in the fit of equation (1) to the observed travel times is about half a millisecond at all three stations (Table 1).

The choice of equation (1) was based on the assumption that the wave speed increases continuously with depth. To test this assumption, a graph of the time interval measured between geophones versus distance for a record close to the shot point was plotted (Figure 6). For reference, the time interval calculated from equation (1) is also shown. If the firn comprised a series of discrete layers, each having a distinct velocity, the graph would appear to be steplike. The plotted points show no evidence of discrete velocity layers, although there are deviations from the smooth curve larger than the reading error that are due, we believe, to lateral inhomogeneities. (The seismogram from which this plot was made is record 21 in Figure 2.)

Once the parameters of equation (1) have been determined, the body wave velocity, v(x), can be found by differentiation. The Wiechert-Herglotz-Bateman (WHB) integral [see Grant and West, 1965] can then be used to find v(z), the velocity as a function of depth, using a numerical program developed by Robertson [1975] [Robertson and Bentley, this volume].

From the P wave velocities the density as a function of depth, $\rho(z)$, can be calculated from Kohnen's [1972] empirical equation:

$$\rho(z) = \frac{0.915}{1 + \{[(v_p)_{max} - v_p(z)]/2250\}^{1.22}} \quad (2)$$

where ρ is in megagrams per cubic meter, the maximum P wave velocity in the ice ($(v_p)_{max}$), is taken to be 3860 m s^{-1}, 0.915 Mg m^{-3} is the density assumed for the depth of the maximum velocity, and $v_p(z)$ is in meters per second. The other constants in equation (2) were derived from refraction velocities and densities measured at Byrd Station on the inland ice sheet of West Antarctica. (Robertson and Bentley [this volume] use $(v_p)_{max}$ = 3850 m s^{-1} instead of 3860 m s^{-1}; the corresponding difference in ρ amounts to no more than 0.003 Mg m^{-3}. See Robertson and Bentley [this volume] for a further discussion.) Kirchner et al. [1979] found good agreement between densities measured directly on cores from a borehole at station J9DS and those calculated from equation (2) for shooting carried out close to the borehole. However, differences as large as 5%, believed to reflect real differences in the ice, were found relative to densities calculated from a refraction experiment carried out only 2 km away from the borehole at station J9DC. The differences in the structure of the firn over such a short distance interval have been attributed by Kirchner et al. [1979] to a remanent effect of a high-stress zone 100 km upstream from station J9DC, through which the ice column passed about 300 years ago.

The travel time to the surface from a charge (0.4 kg) fired in a 8.8-m shot hole at station R16 was used to check the results of the refraction experiment there. The measured time was 5.0 ms, compared with 5.4 ms calculated from the velocities determined by the refraction experiment. The two values are in satisfactory agreement in view of the reading error (0.2 ms) and the fact that the

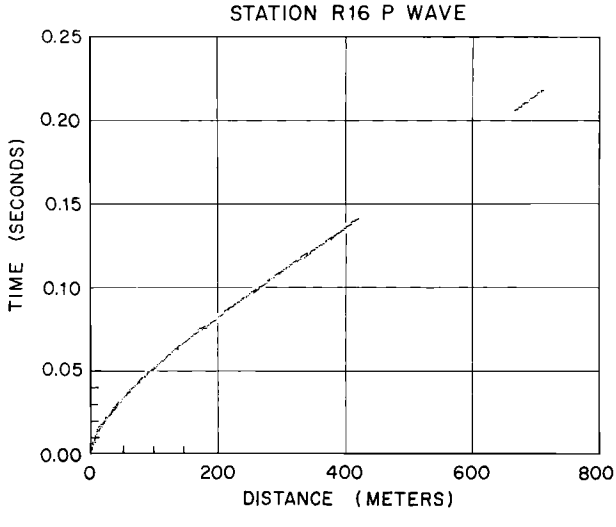

Fig. 5. P wave travel time plot from station R16.

TABLE 1. Least Squares Fit Parameters for the P Wave Travel Time Equation (Equation (1)) for RIGGS IV

Station	n	Maximum Distance, m	t_1, ms	a_1, km^{-1}	t_2, ms	a_2, km^{-1}	v_m, $ms\ km^{-1}$	v_m, $m\ s^{-1}$	Standard Error in t, ms
O11	251	420	22.5	19	8.7	229	267.0	3745	0.5
O19	297	1160	22.9	15	6.3	161	263.5	3795	0.6
R16	331	710	23.6	15	7.1	189	263.7	3792	0.5

Here n is the number of travel time points used in the determination.

hole was sprung (i.e., a charge had already been fired in it), so that the explosive shock wave much have traveled some tenths of meters at high speed.

The maximum velocity measured on each short-refraction profile is given by v_m (Table 1). Previous experience has shown that the true maximum velocity in the ice shelf is not reached until shot-detector distances exceed at least 600 m, and perhaps 1000 m [Robertson, 1975; Robertson and Bentley, this volume]. Only at stations O19 and R15 were those distances exceeded on the short-refraction profiles (except for a shot without a shot break at station O11). The corresponding maximum velocities are 3795 m s^{-1} and 3792 m s^{-1}, respectively. These are slightly less than the average (3811 ± 7 m s^{-1}) calculated for the grid western half of the Ross Ice Shelf by Robertson [1975] [Robertson and Bentley, this volume], but in close agreement with the mean from eight profiles at three RIGGS III stations (3792 ± 16 m s^{-1} [Kirchner and Bentley, this volume]) and with the mean for the whole ice shelf (3790 ± 30 m s^{-1}) calculated from Crary et al. [1962a, Table 7]. As usual, the velocity is much less than that found on the grounded ice sheet at a similar temperature (3850 ± 4 m s^{-1} at -24°C according to Kohnen [1974]). For further discussions, see Robertson and Bentley [this volume].

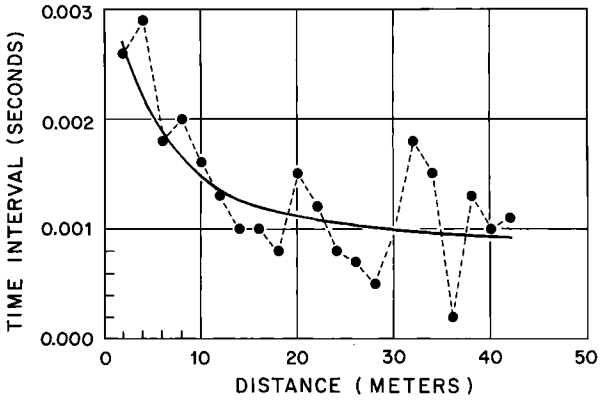

Fig. 6. Travel time interval between geophones versus distance for shot 21 at station R16 (see Figure 2). Solid circles are observed values; the smooth curve is calculated from equation (1).

Another method of measuring the maximum velocity is to calculate the cross-spread velocity on individual shots at sufficiently large distances. This method has the advantage of being unaffected by uncertainties in time breaks and total distances but the disadvantage of providing a determination over only a short distance interval (i.e., the length of the array). When the firn layers are uniform and horizontal, the velocity determinations can be excellent.

The results of this method, which was applied at stations O11, O19, Q13, and R16, are given in Table 2 (the selection criterion was a mean distance greater than 600 m). The means and errors for shots 8-11 at station Q13 and for the separate directions at station O19 were calculated on the assumption that the individual velocities were samples of the same population; the velocities were weighted by inverse variances. The error for station O19, on the other hand, was calculated on the assumption that the single-direction means represent physically different velocities (the first being down dip and the second up dip). Since the profile was not truly reversed, that error cannot be taken as the uncertainty in the determination of the true wave velocity in the ice.

Several conclusions can be drawn from the numbers in Table 2. First, velocities across a spread only 44 m long (shot 53 at station O11 and shot 41 at station R16) are not useful, a fact that is not surprising, since a speed difference of 100 m s^{-1} corresponds to a travel time difference of only 0.3 ms

TABLE 2. Cross Spread P Wave Velocities Determined From Least Squares Analyses of Individual Shots

Station	Shot Number	n	Minimum Distance, m	Spread Length, m	Velocity, m s^{-1}
O11	50	22	593	300	3705 ± 6
	53	23	680	44	3860 ± 50
O19	87N	22	470	690	3784 ± 8
	88N	22	470	690	3776 ± 8
	89N	18	470	690	3789 ± 7
Mean for grid north					3783 ± 5
	91S	21	440	690	3897 ± 9
	93S	20	440	690	3900 ± 12
Mean for grid south					3898 ± 7
Mean for O19					3840 ± 9
Q13	8	12	1110	330	3824 ± 19
	9	12	1110	330	3817 ± 10
	10	12	1170	330	3820 ± 16
	11	12	1170	330	3810 ± 14
Mean for 8-11					3817 ± 7
	69	15	8782	570	3880 ± 32
R16	41	23	666	44	3533 ± 45

N and S denote shots to the grid north and grid south of the spread, respectively; n is the number of travel time points used for each shot.

over a 44-m interval.

Second, it is clear from the shooting in opposite directions at station O19 (even though the profile was not truly reversed) that the constant velocity surfaces are not horizontal there. This was already suspected in the field, because of bending of the ice shelf associated with large bottom crevasses at O19 (S. Shabtaie, personal communication, 1977). A dip of less than 1° (depending on the details of the geometry [see Robertson and Bentley, this volume]) would suffice to produce the observed results. A similar bending caused by bottom crevasses at station O11 is a likely cause of the very low velocity, 3705 m s^{-1}, observed on the unreversed profile there.

Third, the long shot (shot 69) at station Q13 gives a velocity much higher than those measured at 1100 to 1500 m (shots 8-11) on a different spread. Here again we suspect irregularities in the structure, as indicated not only by the high velocity but also by the large scatter of the travel times, which lead to the relatively large standard error in the velocity estimate (±32 m s^{-1}). Observed travel times fall off the least squares regression line by as much as 2 ms, much more than is usually found. Another possible explanation for the high velocity is that the waves are penetrating to an anisotropic layer in which the wave velocity for horizontal propagation is enhanced. A strongly concentrated vertical orientation of crystal c axes could yield a velocity as high as 3880 m s^{-1} [Bentley, 1971]. Gow [1963, 1970] found strongly developed fabrics in the ice cores from Little America V (at the ice shelf front grid south of station Q6 (Figure 1)), but they were characterized by two or more poles offset from the vertical by about 25°, an orientation that would not result in a high horizontal wave velocity. Furthermore, no velocities close to 3880 m s^{-1} were found in

ultrasonic measurements on cores from Little America V [Bennett, 1972; Kohnen and Gow, 1979]. A single-bullseye pattern with most of the axes within 25° of the vertical would be required. Such a pattern is commonly observed on the grounded inland ice, both in Antarctica [Kohnen and Gow, 1979; Russell-Head and Budd, 1979; Korotkevich et al., 1978] and Greenland [Herron and Langway, 1982; Herron et al., 1985] but has not yet been reported in an ice shelf.

Reflections

One of the primary objectives of the RIGGS survey was to measure the ice and water thicknesses over the entire ice shelf on a 55-km (½°) grid. Radar sounding yields a strong reflection from the ice-water interface and is used to measure the ice thickness. However, since radio waves do not penetrate seawater, seismic (acoustic) reflections must be used to measure the depth to the ocean bottom. The two geophysical techniques complement each other, since seismic reflections from the ice-water interface (I_1) are often masked by arrivals propagating along or near the surface of the ice shelf. The difficulty in detecting I_1 is especially great at stations near the edge of the shelf where the ice is relatively thin and the reflection time is short. Most of the stations discussed in this paper were in this area.

The techniques used on the ice shelf differed from those normally used on land in two important respects. First, because the reflections contain such high frequencies, sharp low-cut filters with a -3 dB point at 90 Hz were used to eliminate surface waves (see the section on surface waves below) and to enhance the reflections; high-cut filters were set above 300 Hz or not used at all.

The second major difference was in the use of multiple reflections. Multiples are regarded as a type of noise in most seismic processing, and sophisticated computer techniques have been developed to eliminate them from the seismic records. On the ice shelf, because of the very few reflecting horizons and their high reflection coefficients, multiples not only appear commonly on the seismic records but are easily identified. The multiples thus can be used to confirm the seismic travel times through the ice and water layers found from the primary reflections; this information is especially important in view of the difficulty in detecting I_1. Figure 7 shows ray paths for commonly recorded primary and multiple reflections and gives the nomenclature Crary et al. [1962a] used to label them (see Robertson and Bentley [this volume] for a discussion on how to identify reflection types). A complete seismic record from station P19 and an enlargement of sections of a record from station R17, both showing I_1 and various multiples, are reproduced in Figures 8 and 9. Note the contrast in the appearance between these reflection records and unfiltered records used in refraction and surface wave studies (Figures 2, 3, 11, and 12).

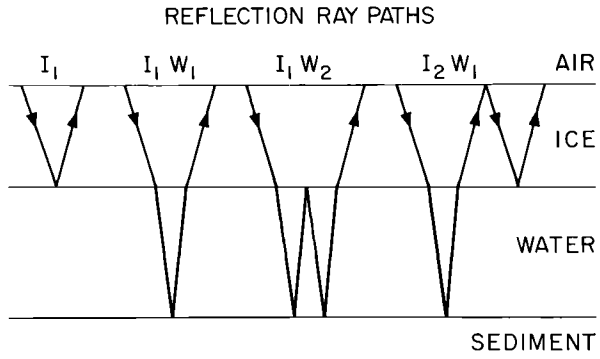

Fig. 7. Reflection ray paths and nomenclature. After Crary et al. [1962a].

Seismic soundings were made at 79 stations during the RIGGS III field season, and 11 more were made during RIGGS IV (Figure 1). To convert the reflection times to layer thicknesses, wave speeds had to be assigned to the ice and the seawater. The sound speed in the water layer was taken to be 1442 m s^{-1}, as calculated by Crary et al. [1962a] from oceanographic data near Little America V. Assigning an average wave speed to the ice was more difficult. Refraction measurements are unsuitable for this because of the temperature-related decrease in velocity below a depth of about 100 m, as pointed out earlier. The average velocity within a layer can be found from the change in reflection time across the detecting spread ("normal moveout") but only if good oblique I_1 reflections are recorded. Robertson [1975] and Robertson and Bentley [this volume] were able to record I_1 reflections clearly enough to use this technique during RIGGS I and RIGGS II at stations on the grid western half of the ice shelf where the ice was relatively thick. Their values for the average speed through the ice shelf, including the upper firn layers, range from 3600 m s^{-1} to 3870 m s^{-1}, with an average of 3688 ± 15 m s^{-1} (corresponding to an average ice thickness of 635 m) for 10 determinations. In the grid eastern half of the ice shelf the ice is thinner; so I_1 is rarely recorded, and even then only poorly.

Since the oblique reflection technique

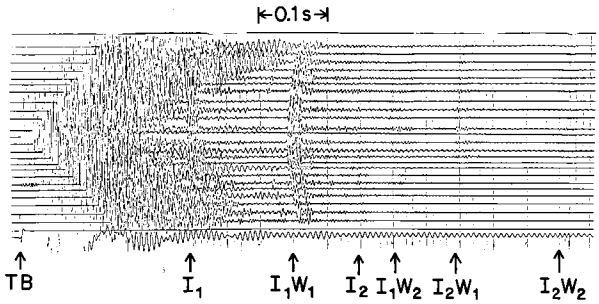

Fig. 8. Sample reflection seismogram (shot 116 from station P19). The energy source was a 150-g charge in a 5-m hole. Geophone spacing was 30 m; 90-Hz low-cut filtering was used. Arrivals are labeled according to Figure 7.

could not be used in our study, a mean vertical velocity was determined indirectly. A vertical travel time of 0.033 s to a depth of 100 m was calculated from the refraction measurements (Table 3). For greater depths a velocity of 3810 m s^{-1} at 100 m [Robertson and Bentley, this volume], a velocity-temperature coefficient of -2.3 m s^{-1} K^{-1} [Kohnen, 1974] and temperature measurements from Crary [1961] and Rand [1975] were used to calculate an average speed below 100 m of 3785 m s^{-1}. Combining these results yielded

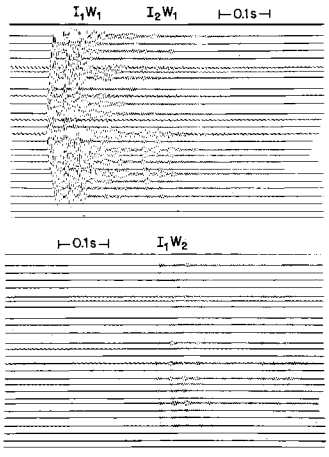

Fig. 9. Enlargement of a reflection seismogram (shot 15 from station R17) showing the bottom reflection (I_1W_1) and the two primary multiple reflections (I_2W_1 and I_1W_2). Note the subbottom reflection that appears 0.03 s after the initial I_1W_1 pulse. The energy source was 150 g in a 5-m hole. Geophone spacing was 30 m; 90-Hz low-cut filtering was used.

TABLE 3. Vertical Travel Time for P Waves to a Depth of 100 m, Calculated From Refraction Shooting

Profile	Travel Time, s	Station Mean
C-16-2	0.0330	0.0330
C-16-3	0.0329	
H13	0.0328	0.0328
J9-1	0.0330	
J9-2	0.0330	0.0329
J9-3	0.0327	
M14	0.0329	0.0329
O11	0.0332	0.0332
O19	0.0323	0.0323
Q13-1	0.0333	0.0332
Q13-2	0.0331	
R16	0.0326	0.0326
Overall mean		0.0328 ± 0.0003

the average velocities through various thicknesses of ice presented in Table 4, which were used to calculate seismic ice thicknesses, h_i(seismic). (These velocities are about 50 m s^{-1} less than those used by Robertson and Bentley [this volume] primarily because of lower velocities very near the surface.)

Radar reflections from the bottom of the ice were recorded at 71 surface stations. At one station where a measurement was not made on the surface, an echo time was taken from airborne sounding on an overflight (station M12), and at one other (station T17S) the ice thickness was extrapolated from a nearby station. Radio echo times in microseconds, t_r, were converted to ice thicknesses in meters, h_i(radar), by the equation $h_i(\text{radar}) = 84.3t_r + 7.6$ [Robertson and Bentley, this volume].

Ice thicknesses (h_i) determined from radar and seismic reflections, water layer thicknesses (h_w), and depths to the seafloor (d_w) at all stations are given in Table 5; a more complete tabulation, including travel times, is given in Appendix B. Both types of h_i values contributed to the map of ice thickness published by Bentley et al. [1979], although that map was based primarily on airborne radar sounding. The ice thickness map, updated along the West Antarctic grounding line (see Robertson and Bentley [this volume]) is reproduced in color in Plate 1. To be consistent, where h_i was measured both by radar and seismic reflections, the latter were used to calculate h_w and d_w. Surface elevations, e, which were needed to obtain d_w, were calculated according to the equation $e = 0.118h_i + 11.6$ m found by Shabtaie and Bentley [1982].

TABLE 4. Calculated Average P Wave Velocities Through the Ice Shelf, as a Function of Ice Shelf Thickness

Ice Thickness, m	One-Way Travel Time, s	Average Velocity, m s^{-1}
250	0.0726	3443
300	0.0858	3495
350	0.0990	3534
400	0.1122	3564
450	0.1254	3587
500	0.1387	3606
550	0.1519	3622
600	0.1651	3635
650	0.1783	3646
700	0.1915	3656
750	0.2047	3664
800	0.2179	3672

A map showing the thickness of the water layer beneath the entire ice shelf, updated from Greischar and Bentley [1980], is reproduced in color in Plate 2.

Direct comparison of actual ice and water column thicknesses with values determined by seismic shooting and by radar is possible at station J9DC because of the hole melted through the shelf during the 1977-1978 season [Clough and Hansen, 1979]. A series of seismic records made during RIGGS III, using a 150-m shot hole, yielded values of 414 ± 2 m and 244 ± 6 m for the ice and water layer thicknesses, respectively. The ice thickness determined by radar was 423 ± 5 m. Measurements in the access hole (T. D. Foster and J. W. Clough, personal communication, 1978) indicate that the ice and water columns are 417 ± 2 m and 240 ± 2 m thick, respectively.

At the 10 RIGGS III stations where h_i(radar) and h_i(seismic) were both found, the difference between them was numerically less than 10 m (Table 5). On the other hand, at the six RIGGS IV stations where both measurements were made (stations P19, Q16, R16, T17, S16, S17), all in the grid southeast corner of the ice shelf, h_i(radar) - h_i(seismic) ranged from 11 to 27 m, with an average of 17 m. Whether this difference is significant as a characteristic of the ice shelf or represents an otherwise unrecognized systematic error in RIGGS IV measurements is difficult to say with so few data. Electromagnetic waves, because of their dependence on the conductive properties of the ice and because their wavelengths are about an order of magnitude smaller than seismic wavelengths (5 m, 3.5 m, and 1.2 m at 35 MHz, 50 MHz, and 150 MHz, respectively, compared with 38 m and 19 m for 100-Hz and 200-Hz seismic waves), are more sensitive than seismic waves to the effect of a transition zone at the base of the ice, such as could be caused by saltwater penetration into the ice or by freezing of seawater on the bottom. However, radar reflection from a transition zone would yield ice thickness values that were too small rather than too large. It is difficult to conceive of a physically realistic model that would incorporate a deeper radar boundary than seismic boundary on floating ice. (Substantially deeper radar reflections were encountered on the grounded ice of Roosevelt Island by Jiracek and Bentley [1971].) As the difference was seen only in RIGGS IV data and not in those from RIGGS III, we must also consider the possibility of a systematic error, even though equipment, procedures, and personnel were the same on RIGGS III and RIGGS IV. If there is an error and it is in the radar measurements, then the same error presumably would apply to h_i(radar) at the other RIGGS IV stations (P18, Q17, Q18, and R18), in which case the water depth at those stations would be some 15 m too great. The uncertainty is not enough to affect materially the maps in Plates 2 and 3.

Using the values of d_w given in Table 5 along with values from other investigations on the Ross Ice Shelf [Crary et al., 1962a, b; Robertson, 1975; M. P. Hochstein and C. R. Bentley, personal communication, 1979], the depth to the ocean bottom beneath the entire shelf was mapped and contoured by Robertson et al. [1982]. Albert et al. [1978] connected that map to maps produced from investigations in the adjacent areas of the open Ross Sea [Hayes and Davey, 1975] and the Rockefeller Plateau [Rose, 1982]. The combined map of the "Ross Embayment" (Plate 3) shows that the region from the continental shelf in the grid western Ross Sea inland beneath the grid western half of the Ross Ice Shelf and for several hundred kilometers inland beyond the grounding line forms a continuous physiographic province with the same average submarine/subglacial elevation over the entire area. The grid eastern section beneath the Ross Ice Shelf and Ross Sea and the deeper lying bed in the grid northwesternmost extremity of the embayment are distinctly different. For further discussion, see Robertson et al. [1982] and Davey [1981].

Seismic reflections from sediments beneath the ocean bottom were recorded at five locations during RIGGS III and IV (a good example can be seen in Figure 9). Unfortunately, because of the short spreads used, it was not possible to determine wave speeds in the sediments by the oblique reflection technique. Another method of estimating wave speeds is

TABLE 5. Ice Thicknesses (h_i), Water Layer Thicknesses (h_w), Depths to the Seafloor, and $\Delta h_i = h_i(\text{radar}) - h_i(\text{seismic})$

Station	Season	h_i(radar), m	h_i(seismic), m	Δh_i, m	h_w, m	Depth to the Seafloor, m Below Sea Level
Q13	III	328	336	-8	445	730
C-16	III	356	356	0	425	727
H13	III	758	NR		502	1159
I12	III	NM	681		126	715
I13	III	NM	460		353	747
I14	III	395	NR		383	720
I15	III	298	NR		588	839
J9DC	III	423	414	9	244	598
J12	III	NM	389		187	518
J13	III	383	NR		298	624
J14	III	410	NR		375	725
J15	III	336	NR		535	820
J16	III	631	NR		175	720
K12	III	408	NR		129	477
K13	III	NM	395		257	594
K14	III	357	NR		373	676
K15	III	368	NR		539	852
K16	III	408	NR		470	818
K17	III	207	NR		500	671
KL7	III	475	NR		250	657
L12	III	NM	395		296	633
L13	III	NM	391		122	455
L14	III	NM	380		229	553
L15	III	328	NR		396	674
L16	III	362	NR		441	749
L17	III	307	NR		376	635
L18	III	391	NR		585	918
L19	III	313	NR		184	448
M12	III	345	NR		364	657
M13	III	NM	368		200	513
M14	III	345	NR		359	652
M15	III	307	NR		432	691
M16	III	NM	393		330	665
M17	III	NM	388		371	702
M18	III	NM	342		505	795
M19	III	NM	292		631	877
N11	III	425	NR		168	531
N12	III	370	371	-1	315	631
N13	III	NM	371		265	581
N14	III	NM	360		450	756
N15	III	NM	366		418	729
N16	III	NM	328		296	574
N17	III	NM	419		362	720
N18	III	NM	395		497	834
N19	III	556	NR		185	664
O11	IV	379	NR		210	533
O12	III	370	NR		293	608

TABLE 5. (continued)

Station	Season	h_i(radar), m	h_i(seismic), m	Δh_i, m	h_w, m	Depth to the Seafloor, m Below Sea Level
O13	III	382	NR		360	685
O14	III	345	NR		458	751
O15	III	379	NR		329	652
O16	III	NM	395		233	570
O17	III	NM	389		363	694
O18	III	NM	482		541	955
O19[a]	III	471	400		493	834
P7	III	345	NM			
P8	III	412	NM			
P9	III	404	403	1	225	569
P10	III	357	NM			
P11	III	383	NR		241	567
P12	III	340	NR		308	596
P13	III	372	NR		405	722
P14	III	319	NR		463	733
P15	III	341	NR		232	521
P16	III	235	NR		353	549
P17	III	416	NR		385	740
P18	IV	412	NR		797	1149
P19	IV	459	447	13	108	491
Q7	III	336	NR		181	466
Q8	III	379	NR		223	546
Q9	III	345	NR		281	574
Q10	III	336	NR		153	438
Q11	III	365	NR		270	580
Q12	III	341	NR		344	633
Q14	III	325	NR		411	686
Q15	III	332	NR		201	482
Q16	IV	395	384	11	582	909
Q17	IV	362	NR		651	959
Q18	IV	509	NM			
R10	III	303	304	-1	188	445
R11	III	293	285	8	322	562
R12	III	315	310	5	375	637
R13	III	302	NR		519	774
R14	III	327	NR		351	628
R15	III	331	NR		501	781
R16	IV	353	342	11	551	841
R17	IV	320	302	18	590	845
R18	IV	218	NR		365	546
S14	III	212	NR		537	712
S15	III	244	NR		604	808
S16	IV	328	306	22	559	817
S17	IV	252	225	27	688	875
T15	III	266	NR		513	736
T17	III	161	NM			
T17S	III	155[b]	NR		739	864

NR, no reflection could be picked; NM, no measurement was attempted.

[a]Station occupied twice; h_i(radar) and h_i(seismic) are not at same spot.

[b]Estimated from station T17, which was 1.6 km away, and the ice thickness gradient.

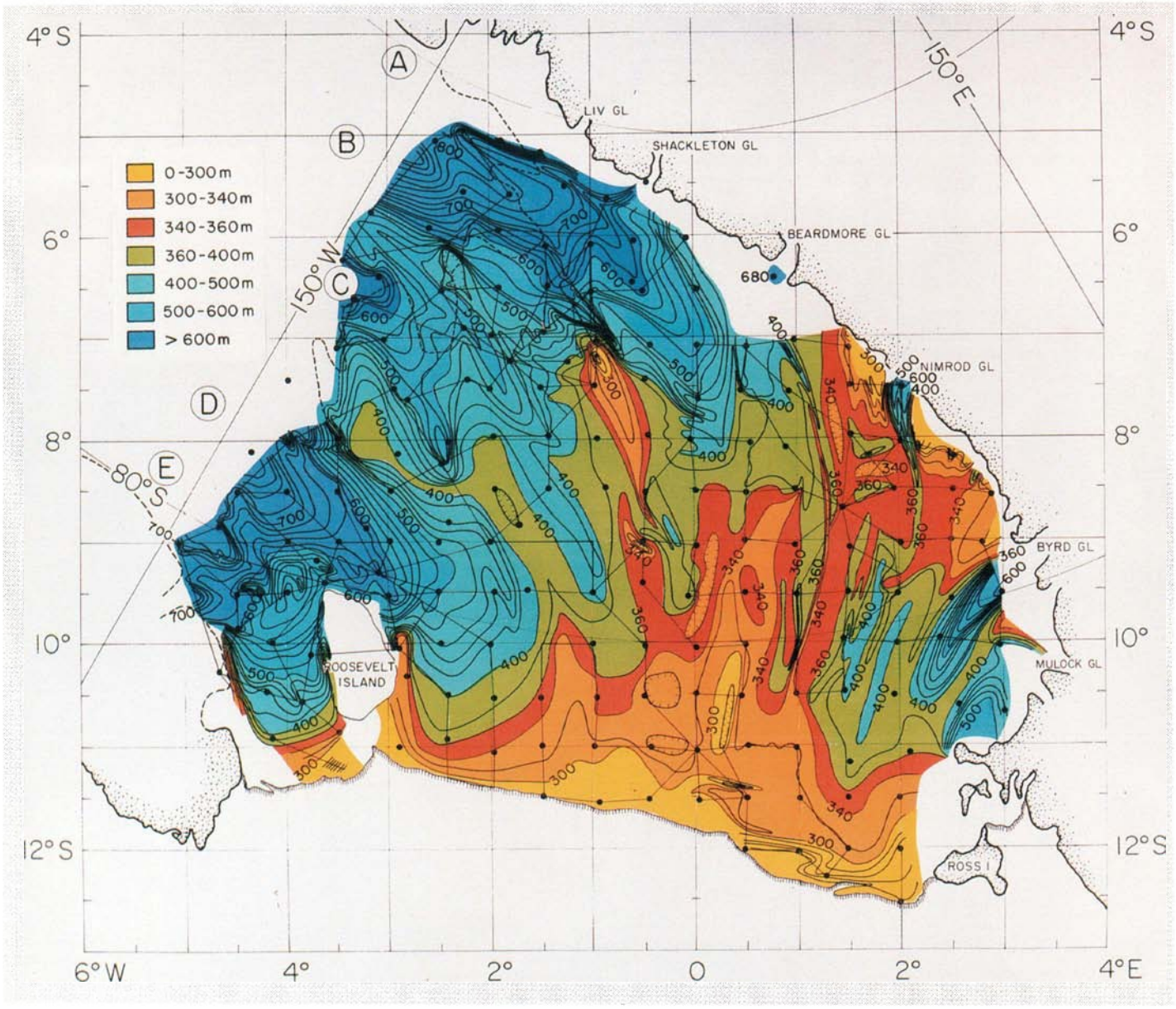

Plate 1. Map of the thickness of the Ross Ice Shelf. Modified from Bentley et al. [1979].

to compare the amplitudes of different reflections. In particular, we may compare I_1W_1 with I_1 to determine the reflection coefficient at the bed, and from that the acoustic impedance in the bed, z_b, using the method described by Robertson and Bentley [this volume]. Unfortunately, only at station P19 were both reflections clear enough and regular enough for a meaningful amplitude ratio to be determined (Figure 8 shows one of the records used at station P19). We find there $z_b = 3.3$ Gg m^{-2} s^{-1}. To get the velocity itself, we have followed Robertson and Bentley [this volume] in using the relationship between density and velocity in continental shelf sediments from Nafe and Drake [1963] and Hamilton [1971, 1982]. The intersection of velocity versus density curves (Figure 10) yields a density of 1.90 ± 0.06 Mg m^{-3} and a velocity of 1.72 ± 0.03 km s^{-1} in the sediment at station P19. (Note that the error estimates do not include a contribution from the uncertainty in z_b, since there was only one measurement of z_b; hence they are surely understated. The errors cited by Robertson and Bentley [this volume] are about twice as great; so to be more realistic, ours have been doubled in the summary and the abstract.) These values are slightly higher than, but in essential agree-

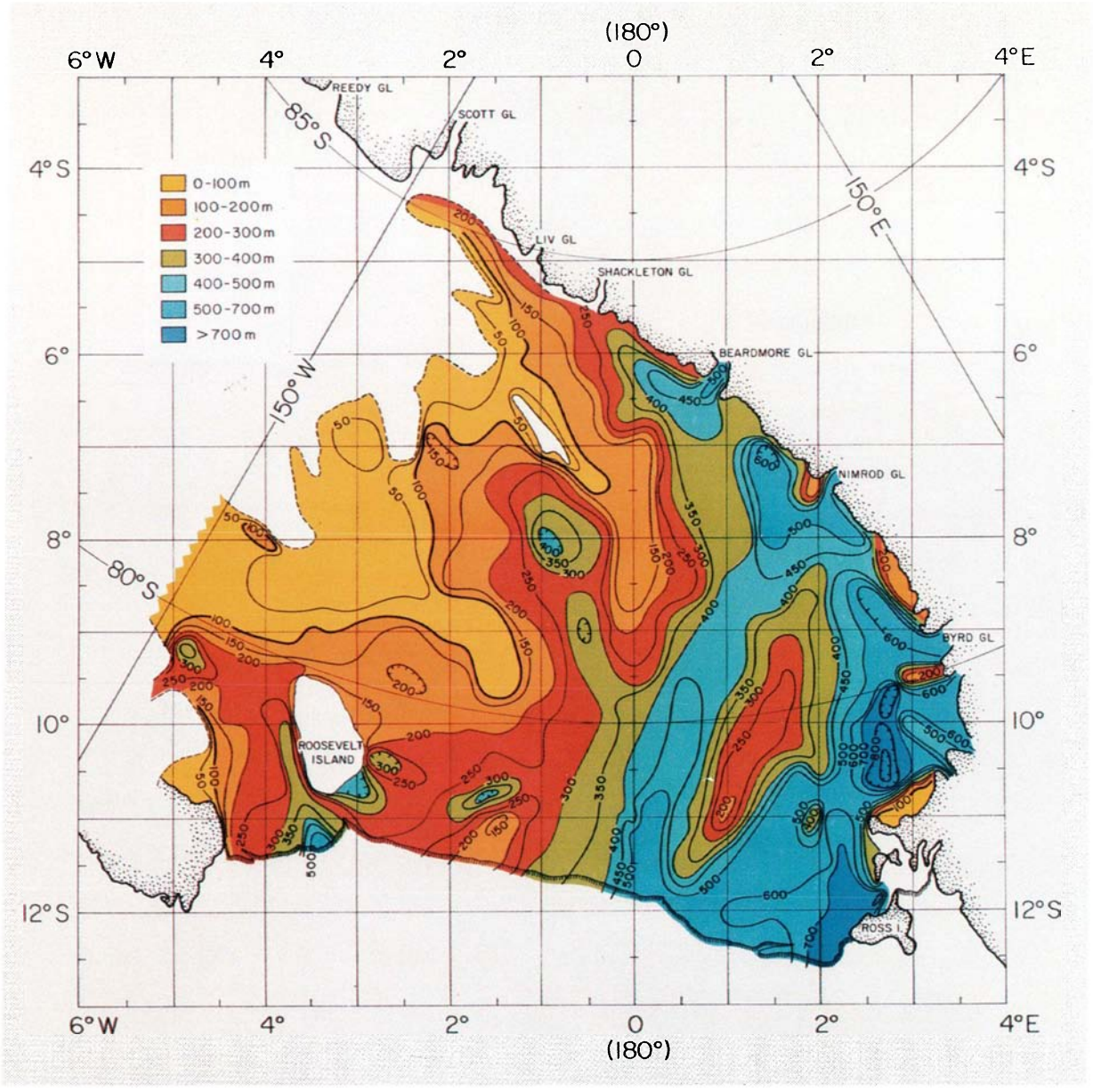

Plate 2. Map of the thickness of the water layer beneath the Ross Ice Shelf. Modified from Greischar and Bentley [1980].

ment with, those of Robertson and Bentley [this volume] for the seafloor beneath the grid eastern half of the Ross Ice Shelf. The velocity value agrees satisfactorily with those measured in the Ross Sea: 1.7 to 2.4 km s^{-1} [Houtz and Davey, 1973; Davey et al., 1983; Cooper et al., 1987].

Surface Waves

A study of seismic surface waves was carried out during RIGGS IV at station Q13. The purpose of this study was to identify the types and modes of surface waves and to examine the dispersion of the waves caused by the change in the elastic parameters with depth in the upper layers of the firn. The dispersion characteristics provide an independent means of checking the velocity structure given by the refraction experiments. Surface wave propagation on the ice shelf and on the polar plateau has been investigated previously by Robinson [1968]. Acharya [1972] and Acharya and Bentley [1978] also have studied dispersion on the polar plateau.

In this investigation the dispersion of both group and phase velocities was determined from the seismograms and compared with values computed from a theoretical model based on the refraction results. The group velocity, U (the speed of energy propagation), and the phase velocity, c (the speed

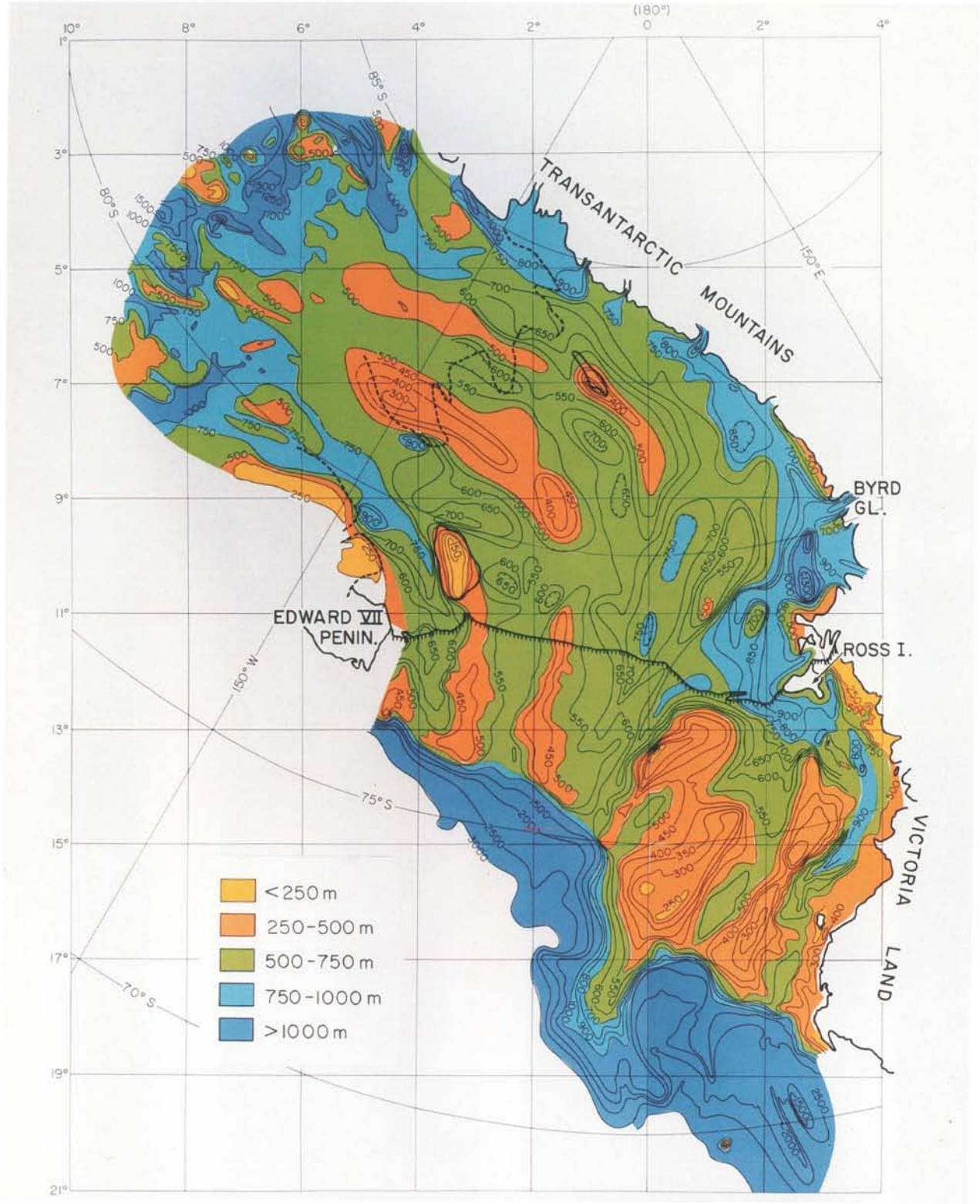

Plate 3. Map of the combined submarine and subglacial topography for the entire "Ross Embayment." First presented by Albert et al. [1978].

of a peak or trough across the spread of detectors), are related by the equation

$$U = c + k \frac{dc}{dk}$$

where k is the wave number.

Surface waves appeared clearly on the RIGGS III refraction records, especially where the shot was more than 1 km from the

spread. Because only vertical component geophones had been used, however, the types of waves could not be identified positively. On the basis of the information from the refraction records, an experiment was designed for RIGGS IV specifically to study surface waves. Horizontal-longitudinal (HL), horizontal-transverse (HX), and vertical (V) geophones all were used in the detecting spread. Charge sizes, shot depths, and shot distances were varied to produce as many different types of surface waves as possible. Table 6 lists the parameters of the shots at Q13 along with the types of waves detected.

First-mode (R_1) and second-mode (R_2) Rayleigh waves were identified on the seismograms (see Figures 11 and 12) by their elliptical motion. The particle motion observed for the first-mode Rayleigh waves was generally retrograde elliptical, but sometimes the ellipse degenerated nearly to a straight line. We suspect minor interference from other wave arrivals, but note that the maximum phase shift was only 90°. With a minimum frequency of 15 Hz and a minimum travel time of 1 s, a 90° phase shift would only cause at most a 2% error in the group velocity. This might be a minor cause of the scatter exhibited in the dispersion data but could not be a source of major error in group velocities. Particle motion at the surface in the second mode is prograde, as expected.

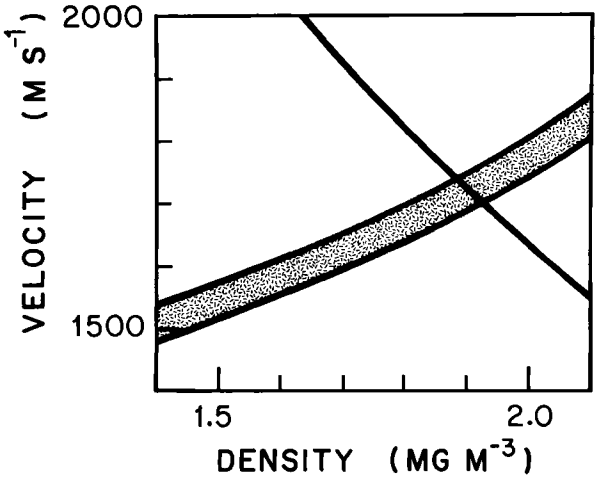

Fig. 10. Plots of velocity versus density in ocean floor sediment beneath station P19. The single curve is the relation found from the measured acoustic impedance; the shaded area denotes the range of values shown by Nafe and Drake [1963] and Hamilton [1971, 1982].

Surface waves with transverse motion, identified as Love waves, also appear on most of the seismic records. Group and phase velocity dispersion curves for all the observed Rayleigh and Love waves are plotted

TABLE 6. Seismic Records Used to Study Surface Waves at Station Q13

Shot Number	Charge, kg	Depth, m	Minimum Distance, m	Spread Length, m	Types of Waves Observed, by Component V	HL	HX
8	1	3	1110	330	R_2	R_2[a]	L
9	1	3	1110	330	R_2[a]	R_2,R_1	L
10	1	5	1170	330	R_2	R_2[a]	L
11	5	5	1170	330	R_2	R_2[a]	L[b]
12	23	5	1170	330	R_1	R_1	L
13	11	3	1140	330	R_2, R_1	R_2, R_1	L
66[c]	5	5	9752	330	PL, R_2	PL	PL
67	39	5	9752	330	PL, R_2	PL	PL
69	380	100	8782	570	PL, R_2	PL	PL

Surface wave types: R_1 and R_2, first and second Rayleigh modes; L, first Love mode; PL, leaky mode.

[a]Superimposed on other modes.

[b]Weak.

[c]All waves very weak.

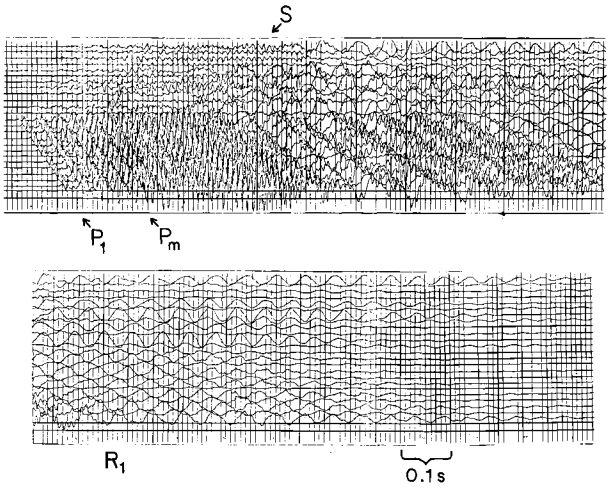

Fig. 11. Seismogram for shot 12 at station Q13; 23 kg in a 5-m hole, 1500 m from the most distant geophones (1 and 24). Geophone spacing: 30 m. Geophone orientations: traces 1, 5, 7, 9, and 11, HL; traces 2, 3, 4, 6, 8, and 10, HX; all others, V. There is a 0.04-s overlap between the upper and lower sections of the record.

in Figures 13 through 16.

Rayleigh and Love waves both propagate at speeds less than that of shear waves. Another wave train, detected from shots at distances of around 10 km, arrives much sooner than the shear wave and only slightly after the compressional wave. We identify these as leaky mode waves [see Laster et al., 1965] that develop from the constructive interference of the low-frequency components of P_m at large m (i.e., a large number of surface reflections) [Robinson, 1968]. Their observed dispersion properties are shown in Figures 17 and 18. Because of the impulsive nature of P_m arrivals for small m, the group and phase velocities of these waves could not be determined until about 450 ms after the first P wave.

The group velocity dispersion is fairly well defined for the leaky mode waves, but the phase velocity dispersion is not. We believe that this stems from the small time differences involved in the passage of these fast waves across the spread, combined with some phase distortion from remaining impulsive P_m arrivals. As no computer program was available to calculate the dispersion of leaky modes, these waves have not been considered further.

A computer program for calculating theoretical Rayleigh and Love wave dispersion curves from a layered model [Dorman, 1962] was used to calculate the dispersion expected from the values of v_p, v_s (two measured curves each for P, SV, and SH), and ρ (calculated from v_p) obtained by short-refraction shooting at station Q13 [Kirchner, 1978; Kirchner and Bentley, this volume] in this volume. The surface waves whose dispersion we measured all had frequencies greater than 13 Hz, corresponding to wavelengths of less than 125 m. As the ice thickness at station Q13 is about 330 m, the effect of the underlying water on the dispersion should be negligible. To check this, we calculated first- and second-mode Rayleigh waves for two models, one with ice and the other with water as the lower half-space, using a program from Herrmann [1978]. There was no difference to the nearest meter per second in phase or group velocities for frequencies greater than 20 Hz for the first mode and 30 Hz for the second mode. At lower frequencies the program failed for technical reasons related to the low wave velocity in the water layer. It is clear, however, that inclusion of a water layer would have no significant effect on the model fitting that we discuss below; so the water was ignored. For the curves presented, 39 layers were used; the layers were 1 m thick down to 30 m, then 5 m thick down to 70 m, with a half-space of ice beneath. Calculations for one particular case showed that using a larger number of layers does not change the calculated results but that 15 layers (all 5 m thick) are too few.

Dispersion curves for first- and second-

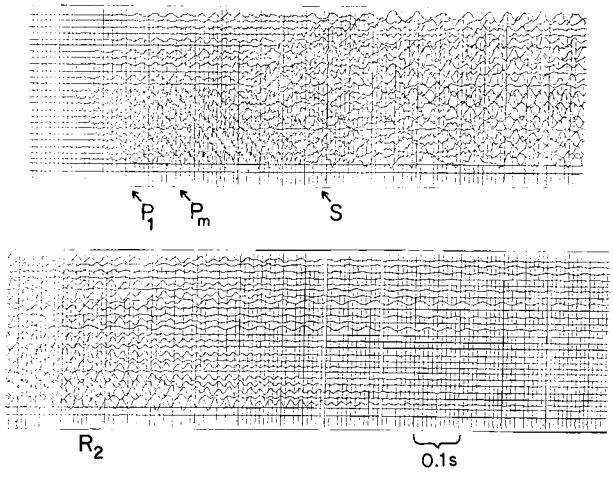

Fig. 12. Seismogram for shot 9 at station Q13. The energy source was a 0.9-kg charge in a 3-m hole, 1440 m from the most distant geophones (1 and 24). Geophone spacing and orientations as in Figure 10. There is a 0.10-s overlap between the upper and lower sections of the record.

mode Rayleigh waves and first-mode Love waves were calculated; they are shown, along with the observed data, in Figures 13 to 16. All models and velocities discussed in this section are tabulated in Appendix C.

The calculated dispersion curves are everywhere higher in velocity than the observed dispersion points. An examination of Poisson's ratio (σ) as a function of depth for the velocities used shows that the values in the upper few meters are certainly incorrect. The values for the first meter are negative, which is physically impossible, and other values at shallow depths are definitely too low. Furthermore, the four curves of σ versus depth (from SV and SH waves each on two different profiles) are widely different in the top 30 m. Three additional models with more reasonable values of σ were therefore investigated. Since the shear wave arrivals can be distorted by P waves and are more difficult than P arrivals to read accurately from the seismograms, we assumed for these models that the P wave velocities are correct; v_s was calculated from the assumed values of σ.

The three new models for v_s, designated A, B, and C, were calculated by assuming that in model A, σ decreases upward from 0.30 to 0.17 in the upper 10 m; in model B, σ is constant at a value of 0.32 in this region, and in model C, σ decreases upward from 0.30 to 0.23. Models A and B represent approximate lower and upper bounds, respectively, to the values of Poisson's ratio found in measurements on polar snow [Mellor, 1964, Figure III-5]. Model C represents reasonable values of σ and is based on the measurements of Thiel and Ostenso [1961] and Kohnen and Bentley [1973]. Only 15 layers (rather than 39) were used in the calculation; the effect of this is to overestimate velocities by an amount that is negligible for phase velocities at the observed frequencies and reaches a maximum of about 100 m s^{-1} for the highest-frequency group velocities.

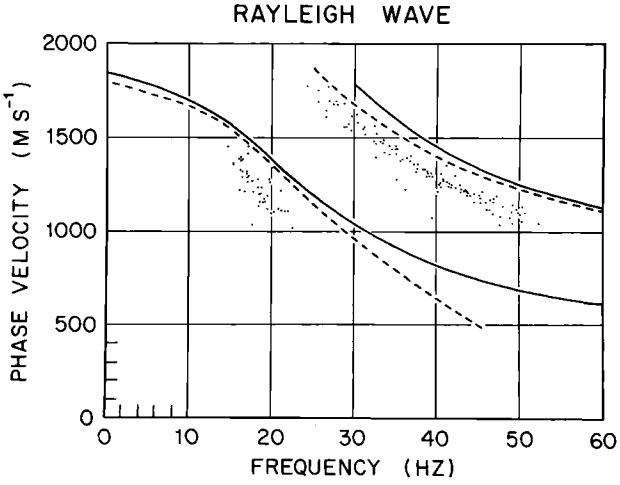

Fig. 14. Rayleigh wave phase velocity dispersion at station Q13, first and second modes. Dots are observed values; lines are calculated according to models SV1 (solid lines) and SV2 (dashed lines).

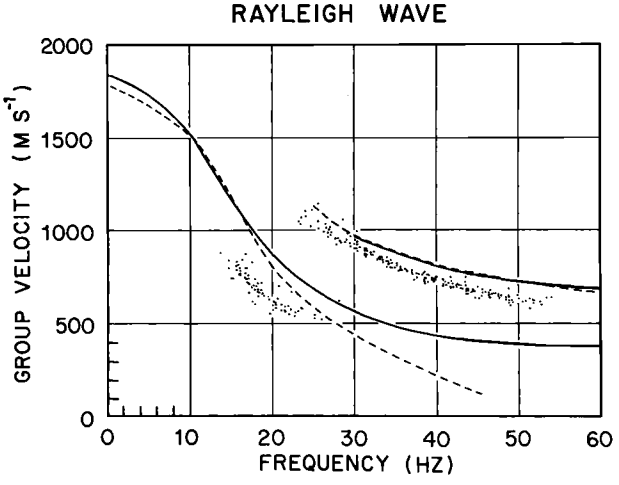

Fig. 13. Rayleigh wave group velocity dispersion at station Q13, first and second modes. Dots are observed values; lines are calculated according to models SV1 (solid lines) and SV2 (dashed lines).

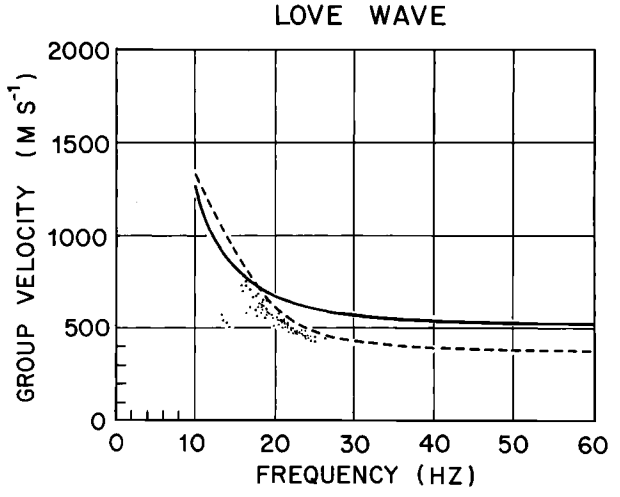

Fig. 15. Love wave group velocity dispersion at station Q13. Dots are observed values; lines are calculated according to models SH1 (solid line) and SH2 (dashed line).

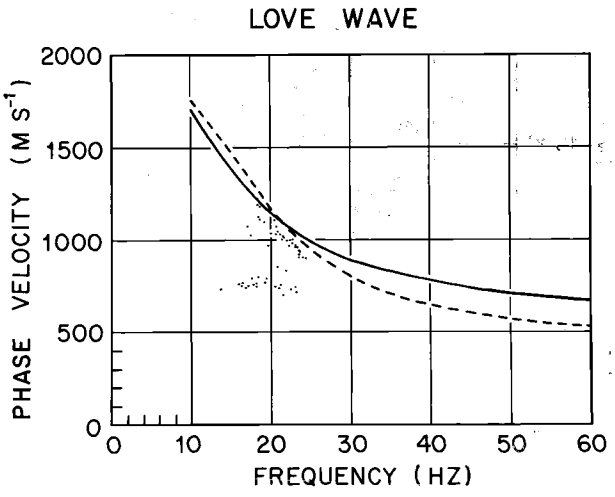

Fig. 16. Love wave phase velocity dispersion at station Q13. Dots are observed values, lines are calculated according to models SH1 (solid line) and SH2 (dashed line).

Plots of the Rayleigh wave dispersion curves calculated using these models (Figures 19 to 24) show a striking change in the second mode, which is much lower in velocity for the new models than for the model based on measured values of v_s. Models A and C both show good agreement with the observed second-mode dispersion. The changes in the first mode are less, since it is less dependent than the higher modes on wave velocities at shallow depths [Kovach, 1978].

These models show clearly how strongly the higher-mode dispersion curves depend on the shear wave velocity in the upper 10 m of the ice. When reasonable velocities are used, good agreement can be obtained between the observed and calculated second-mode Rayleigh wave. Unfortunately, the velocities in the first mode are changed very little in these models. It appears that we must look to a cause other than incorrect v_s in the uppermost firn layers to explain the difference in the first mode between theory and observation.

Robinson [1968] studied surface wave dispersion at four of the sites occupied by the Ross Ice Shelf Traverse (RIST), but only at RIST station C-16 were the shear wave velocities measured at the same site. Geographically, RIGGS station C-16 was about 8 km grid southeast of RIST C-16. Because of ice movement, however, RIST C-16 actually was about 10 km grid southwest of RIGGS C-16 at the time of occupation of the latter. As a check on the comparability of results, we have calculated dispersion curves for RIGGS C-16 using velocities determined by Kirchner [1978] [Kirchner and Bentley, this volume]. Robinson's [1968] and our calculated dispersion curves are in agreement.

Robinson [1968] found a large discrepancy between the observed and calculated dispersion at station C-16, just as we have at station Q13. He also found that assuming an anisotropy in shear wave velocities of 20%, with vertical velocities lower than horizontal velocities, brought the theoretical dispersion curves into good agreement with observations.

We have not calculated dispersion curves for anisotropic models, but we can draw some conclusions by comparing our results with Robinson's [1968]. The observed group velocities for the fundamental mode Rayleigh waves observed at our station Q13 (Figure 12) are essentially identical with those found by

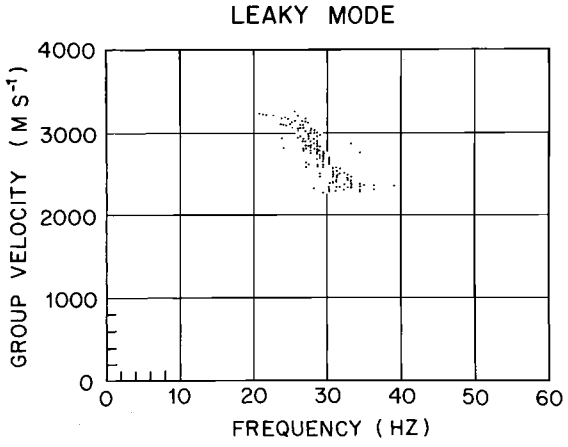

Fig. 17. Observed leaky mode group velocity dispersion at station Q13.

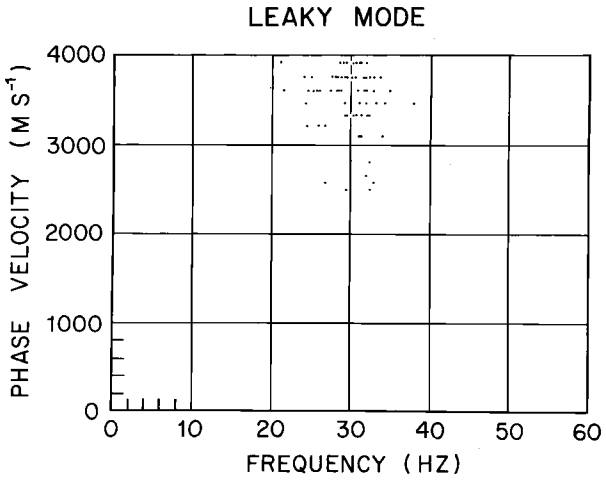

Fig. 18. Observed leaky mode phase velocity dispersion at station Q13.

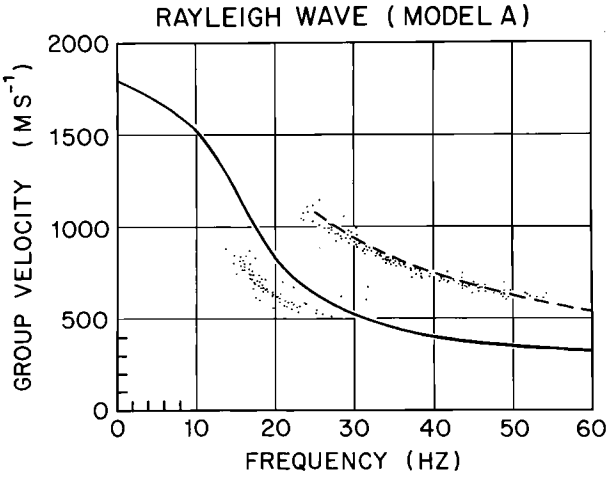

Fig. 19. Rayleigh wave group velocity dispersion at station Q13. Data as in Figure 14. Curves calculated according to model A.

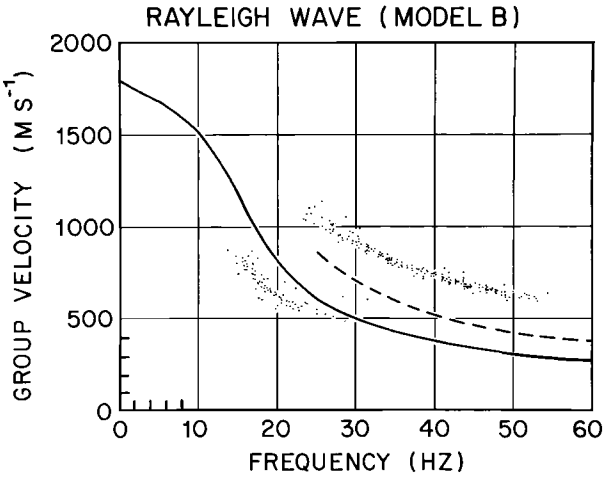

Fig. 21. Rayleigh wave group velocity dispersion at station Q13. Data as in Figure 14. Curves calculated according to model B.

Robinson [1968] for station C-16. The theoretical dispersion curves assuming isotropy (i.e., ours for station Q13 and his for station C-16) are also close to each other. It follows, then, that the 20% anisotropy which he proposed also should bring the theoretical and observed dispersion into agreement at station Q13. If a 20% anisotropy in shear wave velocity exists, it is too large to be the result solely of anisotropy in crystalline structure; it would presumably arise at least in part from the different characteristics of the different layers in the stratigraphic sequence. If we may use crystalline anisotropy as an analogy, however, then it is quite consistent to find low values of v_s associated with normal or even relatively high values of v_p for propagation in the vertical direction [Bennett, 1972], such as those suggested by the uphole time measurement at station R16 (discussed above).

A difficulty that arises with this model is that it could destroy the agreement between theory and observation for the second-mode Rayleigh waves found by correcting Poisson's ratio in the uppermost firn. This problem perhaps can be circumvented by attributing the anisotropy more to the deeper layers, where it could be attri-

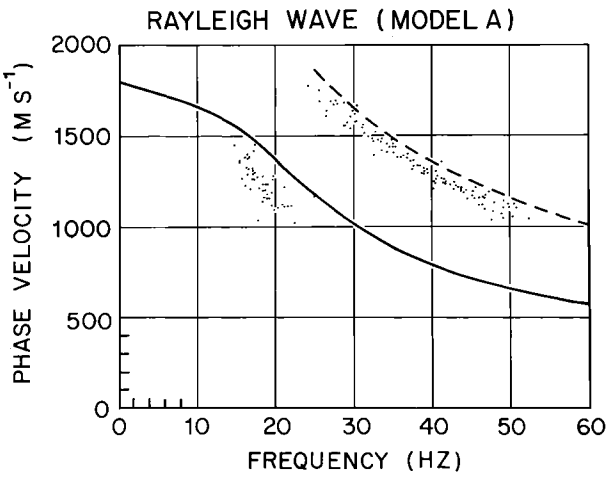

Fig. 20. Rayleigh wave phase velocity dispersion at station Q13. Data as in Figure 15. Curves calculated according to model A.

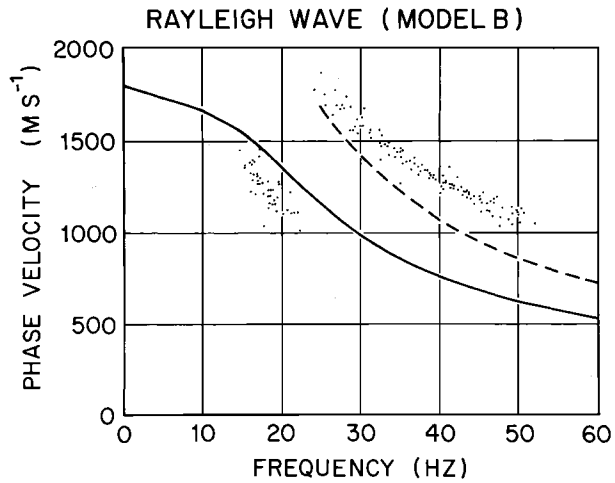

Fig. 22. Rayleigh wave phase velocity dispersion at station Q13. Data as in Figure 15. Curves calculated according to model B.

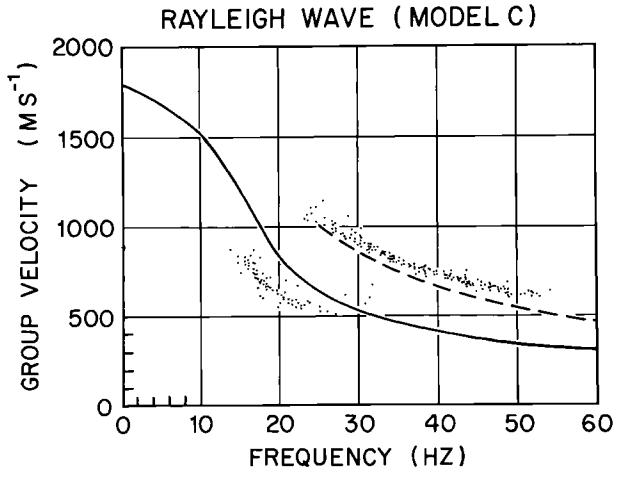

Fig. 23. Rayleigh wave group velocity dispersion at station Q13. Data as in Figure 14. Curves calculated according to model C.

butable partly to crystalline anisotropy [Gow, 1963].

Summary

Inversion of travel time curves from refraction shooting shows P wave velocities that increase monotonically with depth in the upper layers of the ice. The measured P wave velocities at three locations on the ice shelf increase from about 500 m s^{-1} at the surface to about 3800 m s^{-1} at a depth of 60 m. The density as a function of depth at these three locations has been calculated from the P wave velocities using the empirical equation of Kohnen [1972]. Maximum P wave velocities measured at four locations on the ice shelf show a large range of values (3530 to 3900 m s^{-1}) primarily indicative of lateral inhomogeneities (e.g. sloping constant-velocity surfaces) but perhaps also resulting from anisotropy.

The values of ice thickness and water thickness determined from seismic reflection shooting at station J9DC agree very closely with those measured in the access hole there. Water thickness values for 89 additional stations have been determined by reflection shooting, and a bathymetric map of the entire Ross Embayment has been drawn.

Reflection amplitudes were used, along with standard curves of velocity versus density in marine sediments, to calculate a density of 1.90 ± 0.12 Mg m^{-3} and a velocity of 1.72 ± 0.06 km s^{-1} in the uppermost sediment beneath one station (P19).

Rayleigh waves, Love waves, and leaky mode waves were recorded in surface wave experiments at station Q13. An analysis based on measured velocities shows that a layered model, with layers 1 m thick in the upper 30 m and 5 m thick below, suffices for calculating dispersion curves. Theoretical dispersion curves calculated from the measured P wave and S wave velocities give higher values than those observed. An examination of Poisson's ratio as a function of depth reveals errors in the velocities determined by refraction shooting in the upper 10 m of the ice. Correcting those errors by assuming that v_p was measured accurately and taking a reasonable variation in Poisson's ratio bring the calculated and observed second-mode dispersion curves into agreement but have little effect on the first mode. The introduction of S wave anisotropy characterized by a higher vertical than horizontal velocity could bring the observed and calculated first-mode dispersions into agreement.

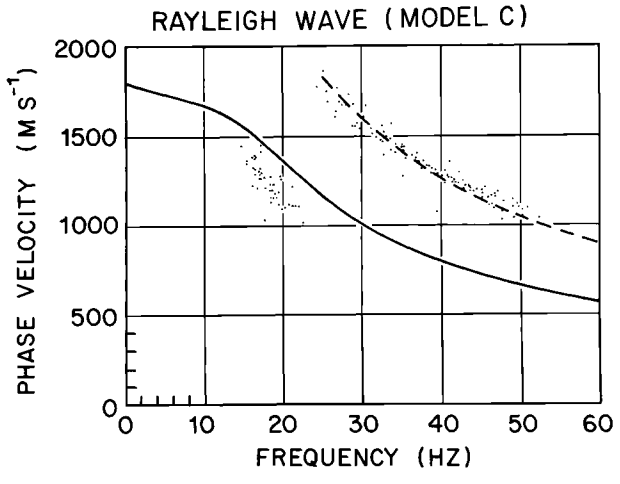

Fig. 24. Rayleigh wave phase velocity dispersion at station Q13. Data as in Figure 15. Curves calculated according to model C.

Acknowledgments. The authors wish to express their appreciation to the other members of the University of Wisconsin field parties, L. L. Greischar, K. C. Jezek, J. F. Kirchner, H. Pollak, and S. Shabtaie, for their aid in all aspects of our work. We are also grateful for the cooperation of members of the groups from the University of Maine, the U.S. Geological Survey, and the University of Copenhagen. Excellent air support in Twin Otter aircraft was supplied by the British Antarctic Survey and Bradley Air Services, Ltd. We thank P. Dombrowski and S. H. Werther for drafting illustrations, and A. N. Mares and J. V. Campbell for manuscript preparation. H. J. Dorman kindly made avail-

able to us the computer program we used to calculate surface wave dispersion. This work was supported by the National Science Foundation under grants DPP72-05802, DPP76-01415, DPP79-20736, and DPP-8119989. This is contribution 435 of the Geophysical and Polar Research Center, University of Wisconsin, Madison.

References

Acharya, H. K., Surface wave dispersion in Byrd Land, Antarctica, Bull. Seismol. Soc. Am., 62, 955-959, 1972.

Acharya, H. K., and C. R. Bentley, Investigation of surface wave dispersion in an inhomogeneous medium by the finite difference method, Bull. Seismol. Soc. Am., 68, 1381-1386, 1978.

Albert, D. G., C. R. Bentley, and L. L. Greischar, Submarine topography of the Ross Embayment from the continental shelf to the Byrd Subglacial Basin (abstract), Eos Trans. AGU, 59, 308-309, 1978.

Bennett, H. F., Measurements of ultrasonic wave velocities in ice cores from Greenland and Antarctica, CRREL Res. Rep. 237, U.S. Army Cold Regions Res. and Eng. Lab., Hanover, N. H., 1972.

Bentley, C. R., Seismic anisotropy in the West Antarctic ice sheet, in Antarctic Snow and Ice Studies II, Antarct. Res. Ser., vol. 16, edited by A. P. Crary, pp. 131-177, AGU, Washington, D. C., 1971.

Bentley, C. R., The Ross Ice Shelf geophysical and glaciological survey (RIGGS): Introduction and summary of measurements performed, in The Ross Ice Shelf: Glaciology and Geophysics, Antarct. Res. Ser., vol. 42, edited by C. R. Bentley and D. E. Hayes, pp. 1-20, AGU, Washington, D. C., 1984.

Bentley, C. R., J. W. Clough, K. C. Jezek, and S. Shabtaie, Ice thickness patterns and the dynamics of the Ross Ice Shelf, J. Glaciol., 24, 287-294, 1979.

Clough, J. W., and B. L. Hansen, The Ross Ice Shelf Project, Science, 203, 433-434, 1979.

Cooper, A. K., F. J. Davey, and J. C. Behrendt, Seismic stratigraphy and structure of the Victoria Land Basin, western Ross Sea, Antarctica, in The Antarctic Continental Margin: Geology and Geophysics of the Western Ross Sea, CPCEMR Earth Sci. Ser., vol. 5B, edited by A. K. Cooper and F. J. Davey, pp. 27-76, Circum-Pacific Council for Energy and Mineral Resources, Houston, Texas, 1987.

Crary, A. P., Glaciological studies at Little America Station, Antarctica, 1957 and 1958, IGY Glaciol. Rep. 5, Am. Geogr. Soc., New York, 1961.

Crary, A. P., E. S. Robinson, H. F. Bennett, and W. W. Boyd, Jr., Glaciological studies of the Ross Ice Shelf, Antarctica, 1957-1960, IGY Glaciol. Rep. 6, Am. Geogr. Soc., New York, 1962a.

Crary, A. P., E. S. Robinson, H. F. Bennett, and W. W. Boyd, Jr., Glaciological regime of the Ross Ice Shelf, J. Geophys. Res., 67, 2791-2807, 1962b.

Davey, F. J., Geophysical studies in the Ross Sea region, J. R. Soc. N. Z., 11, 465-479, 1981.

Davey, F. J., K. Hinz, and H. Schroeder, Sedimentary basins of the Ross Sea, in Antarctic Earth Science, edited by R. L. Oliver, P. R. James, and J. B. Jago, Australian Academy of Science, Canberra, 1983.

Dorman, J., Period equation for waves of Rayleigh type on a layered, liquid-solid half space, Bull. Seismol. Soc. Am., 52, 389-397, 1962.

Gow, A. J., The inner structure of the Ross Ice Shelf at Little America V, Antarctica, as revealed by deep core drilling, IASH Publ. 61, 272-284, 1963.

Gow, A. J., Deep core studies of the crystal structure and fabrics of Antarctic glacier ice, CRREL Res. Rep. 282, 21 pp., U. S. Army Cold Regions Res. and Eng. Lab., Hanover, N. H., 1970.

Grant, F. S., and G. F. West, Interpretation Theory in Applied Geophysics, 583 pp., McGraw-Hill, New York, 1965.

Greischar, L., and C. R. Bentley, Isostatic equilibrium grounding line between the West Antarctic ice sheet and the Ross Ice Shelf, Nature, 283, 651-654, 1980.

Hamilton, E. L., Prediction of in-situ acoustic and elastic properties of marine sediments, Geophysics, 36, 266-284, 1971.

Hamilton, E. L., Sound velocity and related properties of marine sediments, J. Acoust. Soc. Am., 72, 1891-1904, 1982.

Hayes, D. E., and F. J. Davey, A geophysical study of the Ross Sea, Antarctica, Initial Rep. Deep Sea Drill. Proj., 28, 807-907, 1975.

Herrmann, R. B. (Ed.), Computer Programs in Earthquake Seismology, vol. 2, Surface Wave Programs, Publ. 241, Department of Earth and Atmospheric Sciences, St. Louis University, St. Louis, Mo., 1978.

Herron, S. L., and C. C. Langway, Jr., A comparison of ice fabrics and textures at Camp Century, Greenland, and Byrd Station, Antarctica, Ann. of Glaciol., 3, 118-124, 1982.

Herron, S. L., C. C. Langway, Jr., and K. A. Brugger, Ultrasonic velocities and crystalline anisotropy in the ice core from Dye 3, Greenland, in Greenland Ice Core: Geophysics, Geochemistry, and the

Environment, Geophys. Monogr. Ser., vol. 33, edited by C. C. Langway, Jr., H. Oeschger, and W. Dansgaard, pp. 23-31, AGU, Washington, D. C. 1985.

Houtz, R., and F. J. Davey, Seismic profiler and sonobuoy measurements in Ross Sea, Antarctica, J. Geophys. Res., 78, 3448-3468, 1973.

Jiracek, G. R., and C. R. Bentley, Velocity of electromagnetic waves in Antarctic ice, in Antarctic Snow and Ice Studies II, Antarct. Res. Ser., vol. 16, edited by A. P. Crary, pp. 199-208, AGU, Washington, D. C., 1971.

Kirchner, J. F., Seismic refraction studies on the Ross Ice Shelf, Antarctica, M.S. thesis, Univ. of Wis., Madison, Wis., 1978.

Kirchner, J. F., and C. R. Bentley, RIGGS III: Seismic short-refraction studies using an analytical curve-fitting technique, in The Ross Ice Shelf: Glaciology and Geophysics, Antarctic Res. Ser., vol. 42, edited by C. R. Bentley and D. E. Hayes, AGU, Washington, D. C., this volume.

Kirchner, J. F., C. R. Bentley, and J. D. Robertson, Lateral density differences at a site on the Ross Ice Shelf, Antarctica, from seismic measurements, J. Glaciol., 24, 309-312, 1979.

Kohnen, H., Uber die Beziehung zwischen seismischen Geschwindigkeiten und der Dichte in Firn und Eis, Z. Geophys., 38, 925-935, 1972.

Kohnen, H., The temperature dependence of seismic waves in ice, J. Glaciol., 13, 144-147, 1974.

Kohnen, H., and C. R. Bentley, Seismic refraction and reflection measurements at Byrd Station, Antarctica, J. Glaciol., 12, 101-111, 1973.

Kohnen, H., and A. J. Gow, Ultrasonic velocity investigations of crystal anisotropy in deep ice cores from Antarctica, J. Geophys. Res., 84, 4865-4874, 1979.

Korotkevich, E. S., V. N. Petrov, N. I. Barkov, L. I. Suchonosora, D. N. Smitriyev, and V. G. Portnov, Results of the study of the vertical structure of Antarctic ice sheet in the vicinity of Vostok, Antarctica (in Russian), Sov. Antarct. Exped. Inf. Bull., 97, 135-147, 1978.

Kovach, R. L., Seismic surface waves and crustal and upper mantle structure, Rev. Geophys., 16, 1-13, 1978.

Laster, S. J., J. G. Foreman, and A. F. Linville, Theoretical investigation of modal seismograms for a layer over a half space, Geophysics, 30, 571-596, 1965.

Mellor, M., Properties of snow, CRREL Monogr. III-A1, U. S. Army Cold Regions Res. and Eng. Lab., Hanover, N. H., 1964.

Nafe, J. E., and C. L. Drake, Physical properties of marine sediments, in The Sea, vol. 3, edited by M. N. Hill, pp. 794-815, John Wiley, New York, 1963.

Rand, J. H., 100-meter ice cores from the South Pole and the Ross Ice Shelf, Antarct. J. U. S., 10, 150-151, 1975.

Robertson, J. D., Geophysical studies on the Ross Ice Shelf, Antarctica, Ph.D. thesis, Univ. of Wis., Madison, Wis., 1975.

Robertson, J. D., and C. R. Bentley, Seismic studies on the grid western half of the Ross Ice Shelf: RIGGS I and RIGGS II, in The Ross Ice Shelf: Glaciology and Geophysics, Antarct. Res. Ser., vol. 42, edited by C. R. Bentley and D. E. Hayes, AGU, Washington, D. C., this volume.

Robertson, J. D., C. R. Bentley, J. W. Clough, and L. L. Greischar, Sea bottom topography and crustal structure below the Ross Ice Shelf, in Antarctic Geoscience, edited by C. Craddock, pp. 1083-1090, University of Wisconsin Press, Madison, Wis., 1982.

Robinson, E. S., Seismic wave propagation on a heterogeneous polar ice sheet, J. Geophys. Res., 73, 739-753, 1968.

Rose, K. E., High density radio echo sounding of bedrock in Marie Byrd Land, Antarctica, in Antarctic Geoscience, edited by C. Craddock, pp. 985-992, University of Wisconsin Press, Madison, Wis., 1982.

Russell-Head, D. S., and W. F. Budd, Ice-sheet flow properties derived from borehole shear measurements combined with ice-core studies, J. Glaciol., 24, 117-130, 1979.

Shabtaie, S., and C. R. Bentley, Tabular icebergs: Implication from geophysical studies of ice shelves, J. Glaciol., 28, 413-430, 1982.

Thiel, E., and N. A. Ostenso, Seismic studies on Antarctic ice shelves, Geophysics, 26, 706-715, 1961.

(Received December 23, 1987;
revised August 18, 1989;
accepted November 22, 1989.)